OTS PRICE

XEROX $ _2.00 FS_

MICROFILM $ _.50 mF._

A SOLAR ASPECT SENSOR FOR SOUNDING ROCKETS

P. J. McKINNON   L. G. SMITH

CONTRACT NO. NASw-820

PREPARED FOR

NATIONAL AERONAUTICS AND SPACE ADMINISTRATION

HEADQUARTERS

WASHINGTON 25, D. C.

JULY 1964

GEOPHYSICS CORPORATION OF AMERICA   BEDFORD, MASSACHUSETTS

A SOLAR ASPECT SENSOR FOR SOUNDING ROCKETS

P. J. McKinnon
L. G. Smith

July 1964

ABSTRACT

This paper contains a detailed description of a solar aspect sensor, the operation of which is dependent on a silicon solar energy convertor. Special attention is given to the reasons that led to the choice of a photo-voltaic device for the application and to the analysis of the geometry by which the aspect concept is realized. Some comparisons with the earlier version of the solar aspect sensor are made to indicate the improvements. The instrument measures the angle between the spin axis of the rocket and the sun-rocket line for angles between 20° and 160° with an accuracy of $\pm 1^{\circ}$.
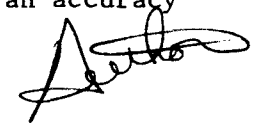
i

TABLE OF CONTENTS

LIST OF ILLUSTRATIONS

INTRODUCTION

The solar aspect sensor has been designed to measure the angle between the longitudinal axis of a spin-stabilized rocket and the direction of the sun. Its primary purpose is to provide aspect data to correct the measured response of solar radiation detectors to conditions of normal incidence.

The technique involves a diamond-shaped aperture with a light detector placed a fixed distance behind the center of the aperture. The sensor is mounted with the long axis parallel to the spin axis of the rocket. As the rocket spins, the detector, indicating the intersection of the sun-detector line and the aperture, functions as an off-on switch. The aspect angle is obtained from the time interval between two pulses generated in the device by the spin of the rocket.

The earlier version of the solar aspect sensor (Model XAS-101) used a photo conductive silicon diode (Texas Instruments, IN2175) as the light detector. The improved sensors (Model XAS-102) makes use of a photo-voltaic silicon device (Solar Systems, SS-30). The features that a solar energy convertor provide for this application greatly minimize the major shortcomings of the original sensors — the time and complexity of the calibration procedure.

In addition to its primary purpose, the instrument provides valuable information on vehicle motion. The most readily determined value is spin rate. The included angle and period of the precession cone is also obtained. The data of some recent flights is shown in the final section to indicate how these results are obtained.

The aspect sensor has been successfully flown on Nike-Apache rockets in support of X-ray Geiger counters and Lyman-α ion chambers.

GENERAL THEORY OF SOLAR ASPECT SENSOR

The intersection of the plane containing the diamond-shaped aperture and the cone generated by the sun-detector line as the rocket spins about its longitudinal axis is illustrated in Figure 1. The plane, parallel to the rocket spin axis, is a distance d from the detector. The detector is assumed to be located on the spin axis since all points in a rigid body have equal angular velocity. The equation of the line of intersection is a hyperbola given by the simultaneous solution of the right circular cone.

$$a^2x^2 + a^2y^2 = z^2$$

and the plane

$$x = d$$

Substituting,

$$z^2 - a^2y^2 = a^2d^2 .$$

Solving for the constant, a, at the point $y = 0$, $z = d \tan \alpha$

$$a = \tan \alpha$$

Hence

$$z^2 - \tan^2\alpha y^2 = d^2\tan^2\alpha \qquad (1)$$

A detailed view of the geometrical arrangement of the diamond-shaped aperture and light detector is shown in Figure 2. The detector is located at O, a distance $d = OP$ behind the center of the aperture. The size of the aperture, ABCD is determined by the distance d and the two angles,

$$BOP = \alpha_m$$

and

$$AOP = \phi_o$$

where α_m is the maximum aspect angle and $2\phi_o$ is the maximum azimuth angle.
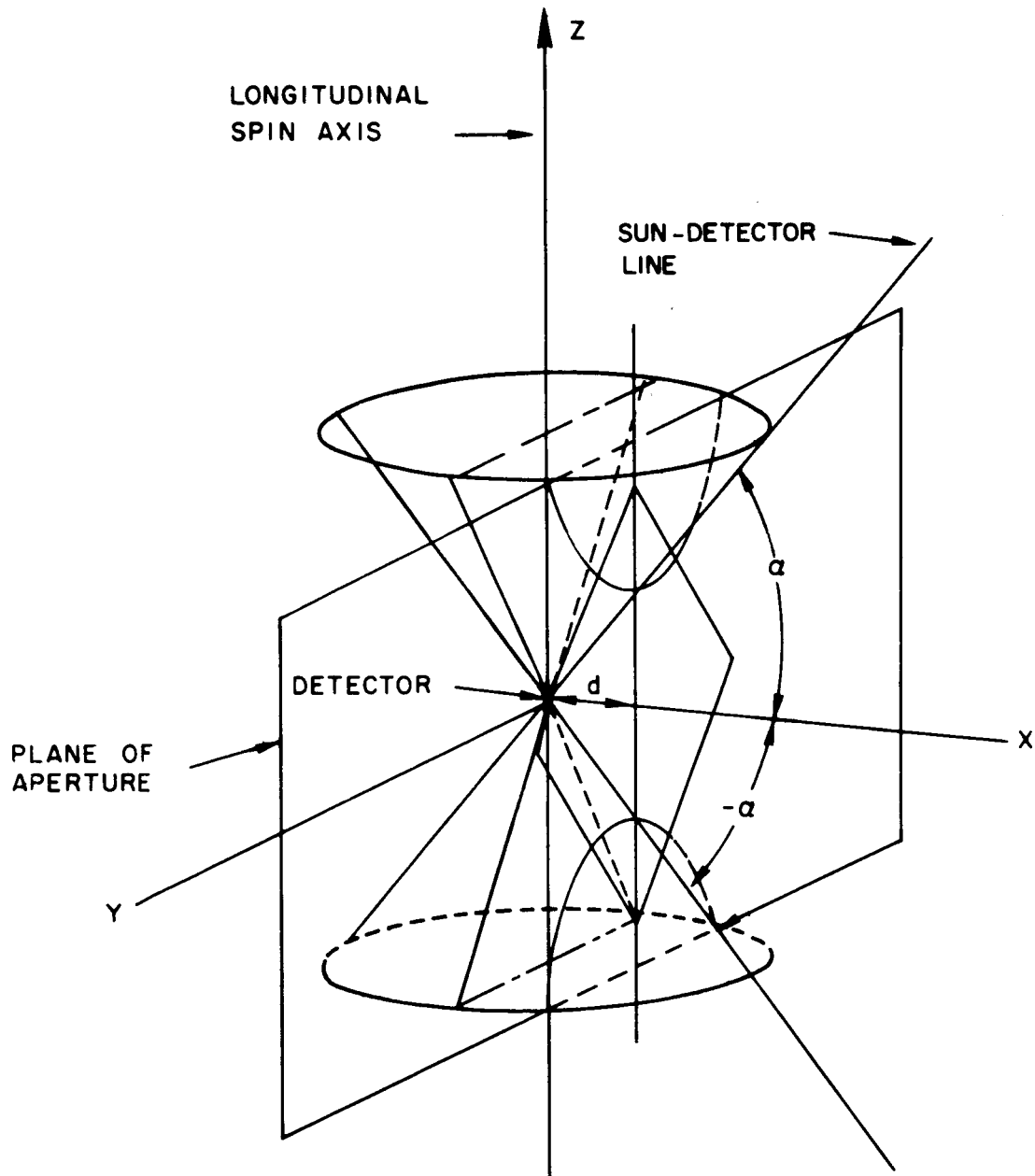
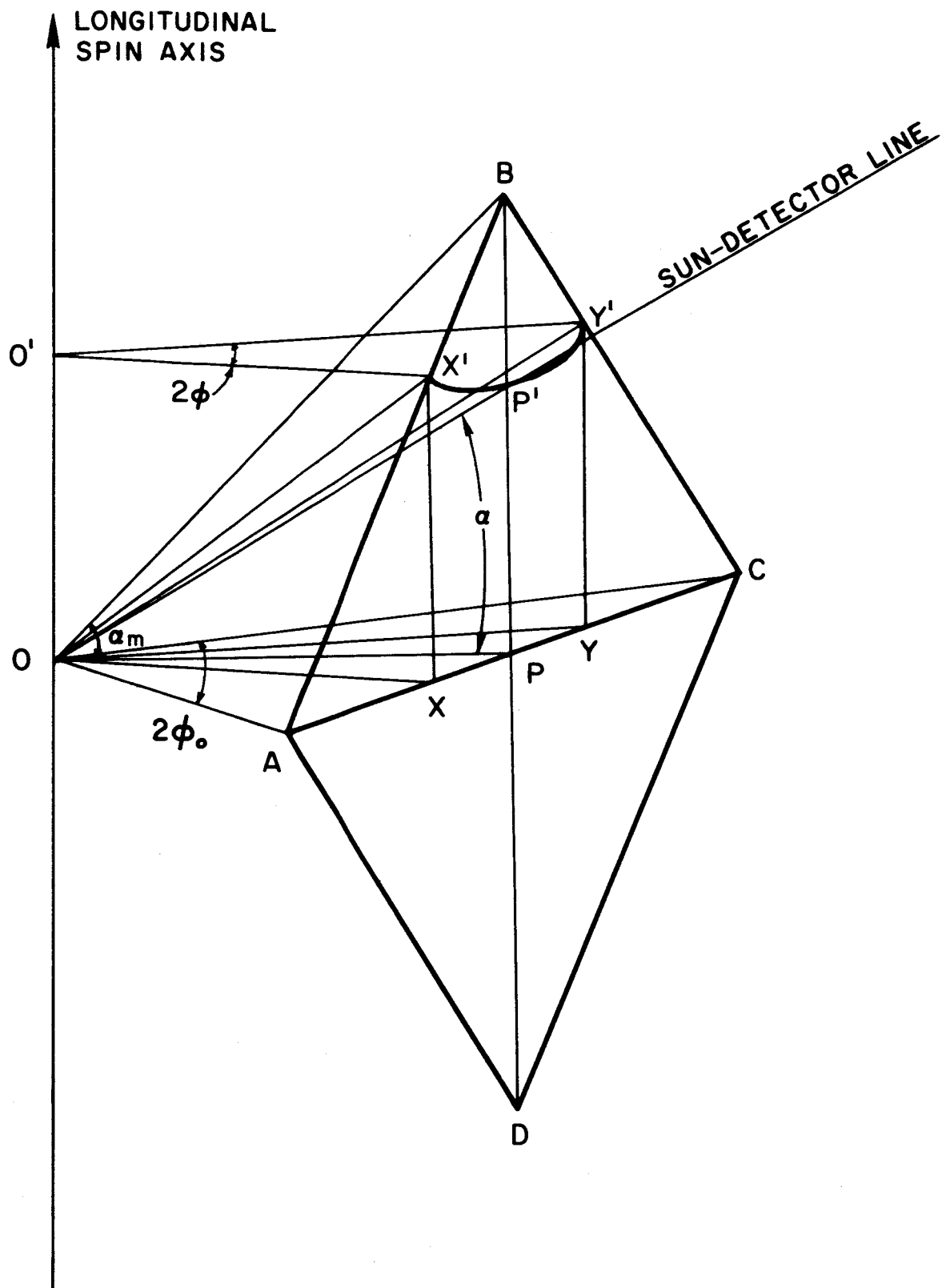Figure 1. Intersection of cone and plane of aperture.

Figure 2. Geometry of solar aspect sensor.

By substituting $y = XP = d \tan \phi$ into equation (1) the result is

$$z = XX' = d \sec \phi \tan \alpha$$

Since

$$OX = d \sec \phi$$

then

$$\tan XOX' = \tan \alpha$$

So

$$XOX' = YOY' \equiv \alpha \ .$$

The time interval between X' and Y' is determined by the angular velocity of the rocket and the angle

$$X'O'Y' = 2\phi \ .$$

This azimuth angle is completely determined by the aspect angle α and the two fixed angles α_m and ϕ_o.

Now

$$AP = d \tan \phi_o$$

$$BP = d \tan \alpha_m$$

$$AX = d \tan \phi_o - d \tan \phi$$

$$XX' = d \sec \phi \tan \alpha \ .$$

By similar triangles $AX'X$ and ABP,

$$XX'/BP = AX/AP$$

whence

$$\tan \alpha = (\cos \phi - \sin \phi \cot \phi_o) \tan \alpha_m$$

$$(2)$$

For purposes of data analysis, this equation is plotted in the form of ϕ/ϕ_o versus α in Figure 3 for $\phi_o = 60^\circ$ and $\alpha_m = 70^\circ$.

The accuracy of the device is determined by two main factors: (1) the mechanical tolerance of the components that fix the geometrical configuration and (2) the time measurement of the telemetry
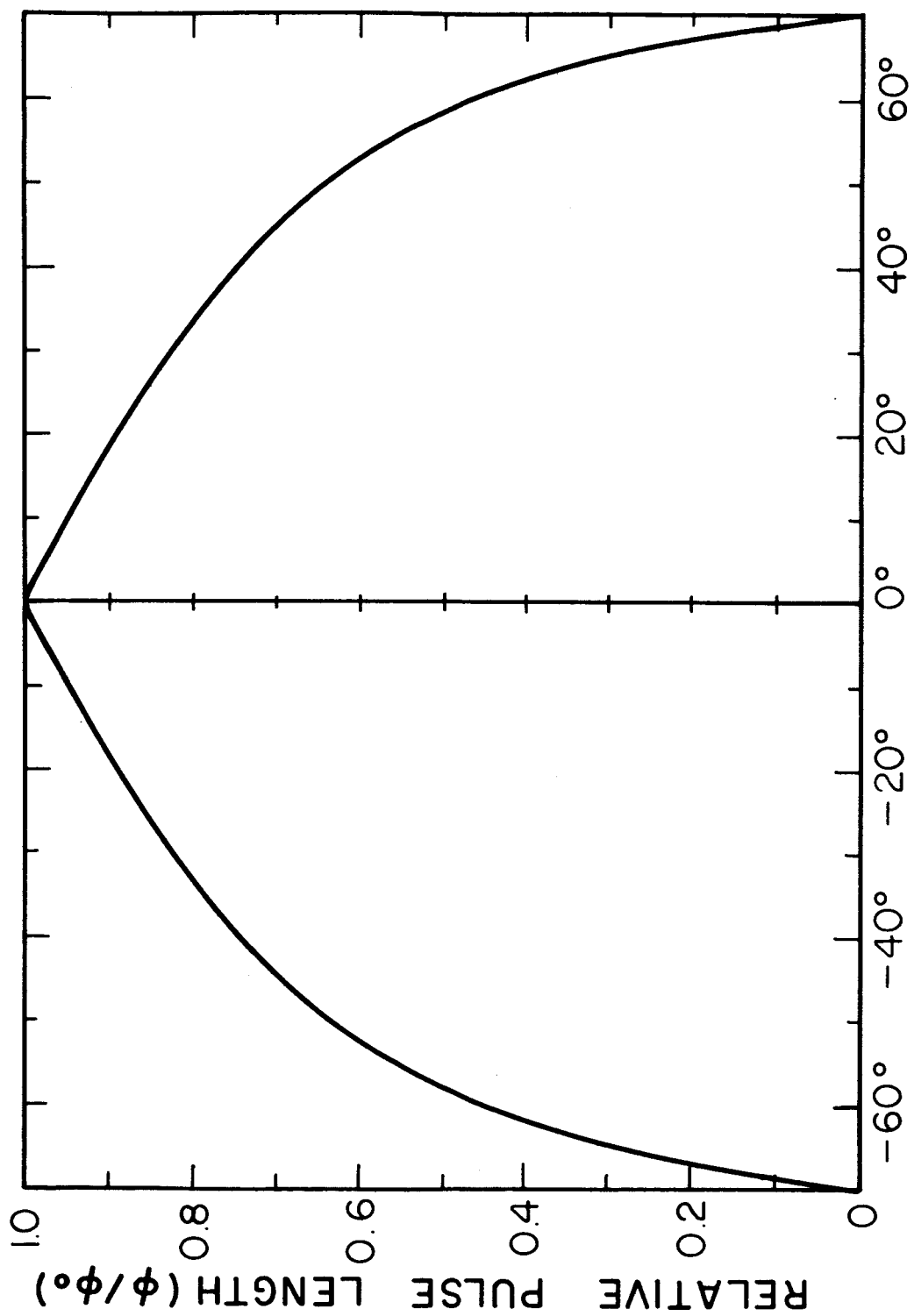
6

Figure 3. Calibration curve of aspect sensor

record. An analysis of the errors introduced by mechanical toler-
ance was performed. The results were used to set tolerances such
that the maximum error in α is less than 0.3°.

The time measurement error is that results of a reading error
and the geometrical arrangement as given by Equation (2). Figure 3
shows that the device is least sensitive near $\alpha = 0^{\circ}$, that is, with
the rocket longitudinal axis perpendicular to the direction of the
sun, and becomes more sensitive as the aspect angle increases. This
is advantageous in practical applications since it complements the
aspect sensitivity of the solar radiation sensor with which it has
normally been used.

Near $\alpha = 0$, the linear part of the calibration, the change in
α for a change in ϕ may be written:

$$\delta\alpha = -\frac{\tan \alpha_m}{\sec^2\alpha} [\sin \phi + \cot \phi_o \cos \phi] \delta\phi$$

Now

$$\frac{\phi}{\phi_o} = \frac{t}{t_o}$$

where t is the time interval at aspect angle α and t_o is the time
interval at $\alpha = 0^{\circ}$.

Hence

$$\delta\phi = \frac{\phi_o}{t_o} \delta t.$$

Thus, the error $\delta\alpha$ in α resulting from an error in δt in t is
given by

$$\delta\alpha = -\frac{\phi_o \tan \alpha_m}{t_o \sec^2\alpha} [\sin \phi + \cot \phi_o \cos \phi] \delta t$$

For the actual case of a 5 rps spin rate and the particular
values of ϕ_o and α_m given above,

$$t_o = 200 \times \frac{120}{360} = 67 \text{ ms.}$$

It is reasonable to measure the time interval of 0.5 ms on a
10 in/sec telemetry record. Therefore for $\delta t = 0.5$ ms, the corres-
ponding error in α is about 1°. This represents the probable read-
ing error in measurement of aspect angles up to about 30°. Beyond

8

this the accuracy increases continuously to a theoretical value of 0.1° at the limit of the sensor, $\alpha = 70^{\circ}$.

The diamond shaped aperture and output signal are shown in Figure 4. The simple diamond shaped aperture is ambiguous with respect to positive and negative aspect angles. The output signal is coded by adding a third pulse for positive angles. Also, the aperture has been modified to include additional markers at 0°, $\pm 30^{\circ}$, and $\pm 60^{\circ}$ aspect angle to complement the theoretical calibration with an in-flight calibration. The occurrence of the in-flight calibration is assured even in a well stabilized flight, since the rocket will turn over on descent from a nose up attitude to a nose-down attitude in the altitude range 100 km down to 70 km. This point is illustrated in Figure 13 for the flight of the Nike-Apache 14.143.

α (POSITIVE)

α = 0°

α (NEGATIVE)
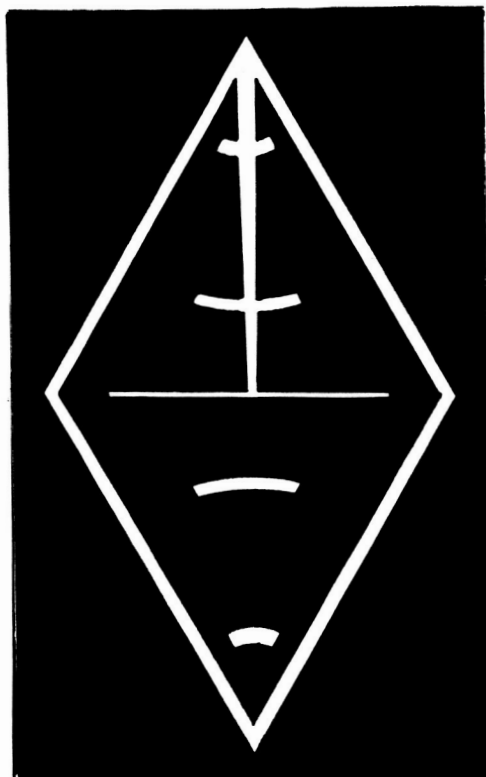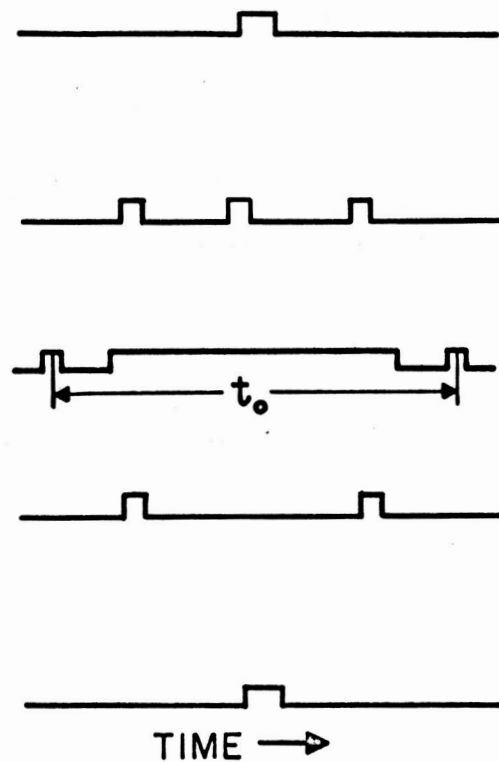
(a)　　　　　　　　(b)

Figure 4.　(a) Diamond-shaped aperture and
(b) Output signal

APPLICATION OF SOLAR ENERGY CONVERTOR AS LIGHT DETECTOR

The original series of aspect sensors (Model XAS-101) used a photoconductive silicon diode (1N2175) as the light detector. Although its accuracy was entirely satisfactory, the sensor required a painstaking, expensive calibration procedure. The recent design review pointed to the physical characteristics of the package embodying the semiconductor as the major source of difficulty in using the photodiode for this application.

The semiconductor, encased in a cylindrical package, is exposed to light by a lens which limited the angular range to 10 degrees. Its use in the aspect sensor required a large angular range of exposure. The angular range of the diode was extended to almost 90 degrees by roughening the surface of the lens. Because of surface irregularities resulting from the grinding process, the lens did not transmit light equally well from all azimuth angles for a given aspect angle.

It is noted in Figure 2 that the light detector is illuminated by light entering the aperture slits at angles greater than 50 degrees for any aspect angle. Although the photocurrent increases linearly with illumination its variation with angle is much more drastic. The photocurrent at angles greater than 50 degrees is at least two orders of magnitude lower than that of normal incidence. Consequently, the threshold of the switching circuit must be set to make the photodiode sensitive to signal light entering at wide angles and, yet, insensitive to scattered or background light entering at normal incidence. Ideally, the threshold should be such that the ratio of photocurrent at onset to bias current is a maximum. The ratio is somewhat reduced for calibration purposes since scattered and background light combine to produce a photocurrent which must be offset by increased bias current.

Because of the shortcomings of the grinding process, the weaker response of the detector at wide angles, and any additional mechanical errors introduced in mounting the cylindrical package, the actual switch-on points did not accurately conform to those determined by the geometrical configuration. For these reasons, a thorough point-by-point calibration of each aspect sensor was required to establish a reliable calibration curve for use in data reduction.

The new aspect sensor uses a silicon solar energy convertor as the light detector. The photovoltaic device has two distinct advantages over the photoconductive unit that make it more applicable

for the aspect sensor, namely, (1) the output voltage is approximately proportional to the cosine of the angle of incident light and (2) for small areas, the output voltage is a function of total area exposed. In designing the aperture plate, the area factor can be adjusted to largely counteract the cosine dependence, consequently, the output voltage of the cell is nearly independent of aspect or azimuth angle.

The solar energy convertor (SS-30) is a flat disk, about 1 inch diameter with a conversion efficiency of approximately 10 percent. In the aspect sensor the cell is exposed to light over a small circular area, 0.1 inch diameter. Tests were conducted to determine the variation in output voltage as a function of (1) area and (2) temperature.

The results are shown in Figure 5. The output voltage increases linearly as a function of area with 7.85×10^{-3} square inch taken as the 100% value of active area. The area factor is exploited by increasing the width of the aperture slits from 0.020 inch to 0.040 inch for angles greater than 30°. The aspect sensor in the Nike-Apache 14.143 payload was instrumented to measure the analog voltage of the solar energy convertor. The data indicated that the output voltage at an angle of 60° was only 7% less than the value at normal incidence due to the area compensation.

The temperature tests were conducted to determine if any significant change in temperature coefficient resulted from the unusual restriction imposed on the photosensitive area. An area approximately 2.8×10^{-3} square inch was illuminated by a tungsten source. The tests covered a temperature range of 0°F to 150°F in which the initial output voltages at 75°F varied from 200 to 350 millivolts for fifteen samples. The initial voltage for each cell was determined from sensitivity measurements made in direct sunlight at 75°F. The results indicate a linear decrease in output voltage as a function of temperature with an average slope of -1.3 mv/$^{\circ}$F, a value typical of silicon.

A second group consisting of samples of reduced sensitivity were similarly tested. The initial output voltages ranged from 110 to 150 millivolts at 75°F. These units at low temperatures showed the same average slope of -1.3 mv/$^{\circ}$F, but the slope decreased with increasing temperature over the range of 0°F to 150°F. To satisfy the requirements imposed by the use of solar energy convertors of different sensitivities, the problems of temperature compensation of the threshold bias of Q_1 were readily solved by using a resistor-silicon diode voltage divider to provide bias voltage as indicated in Figure 6, the schematic of the switching circuit. The effect of temperature on the switching circuit is shown in Figure 7. This
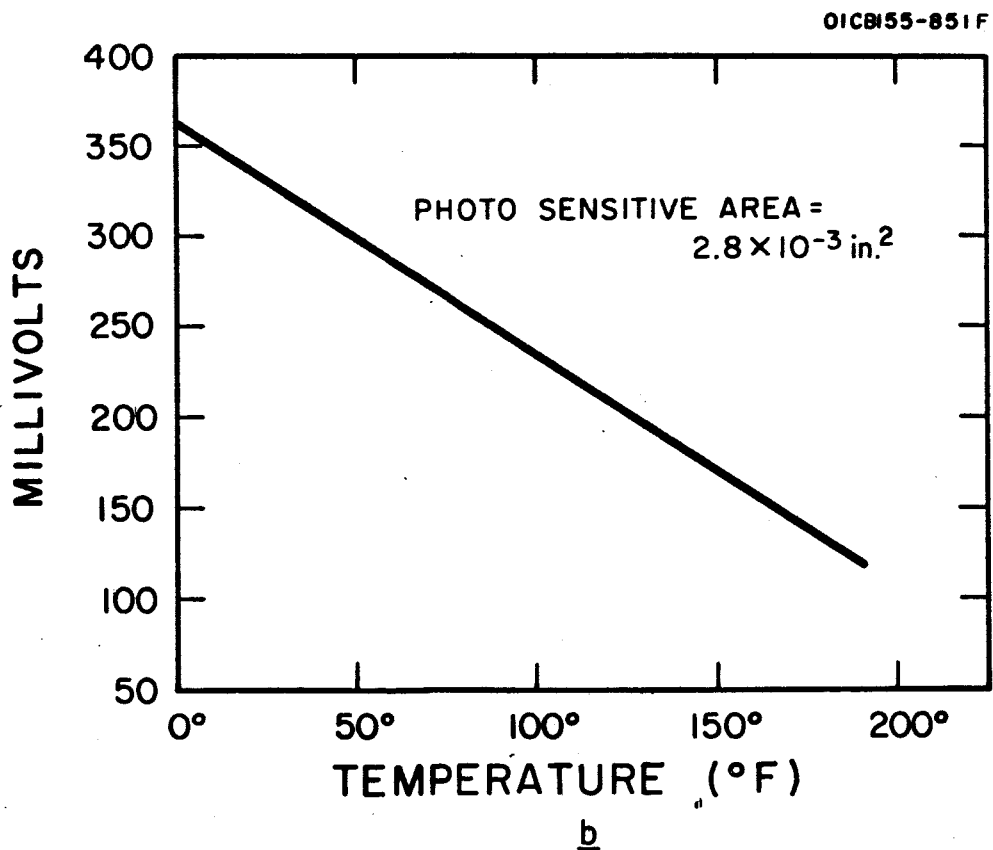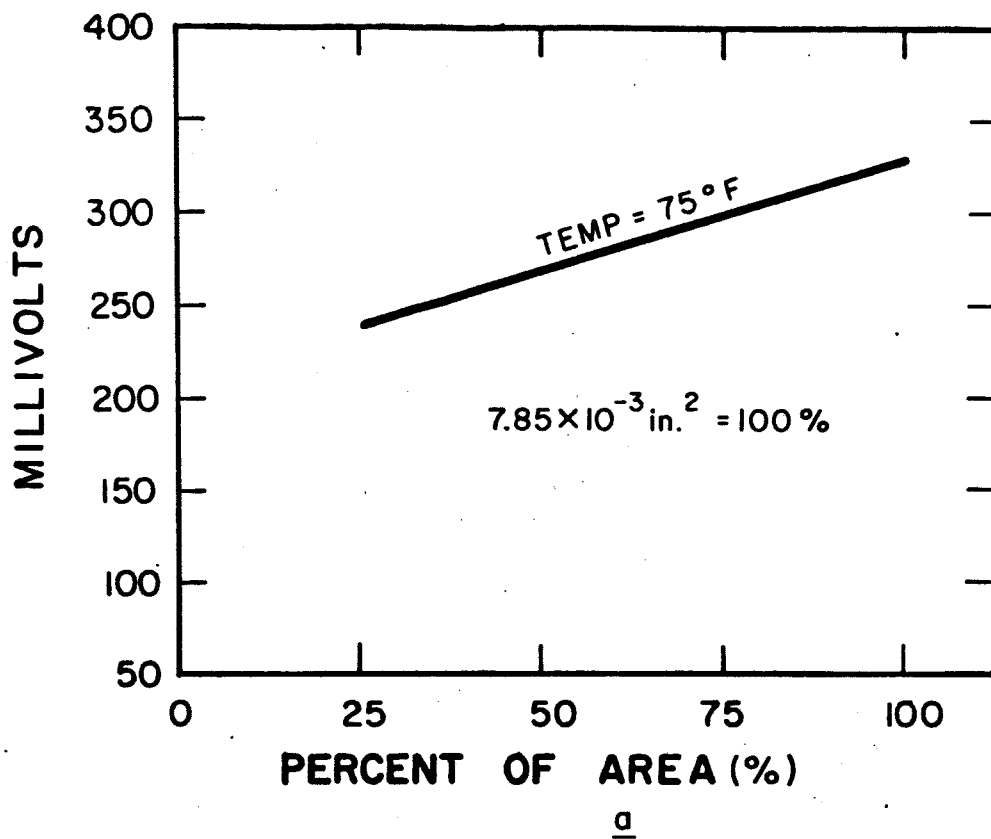
Figure 5. Output voltage of silicon solar energy convertor
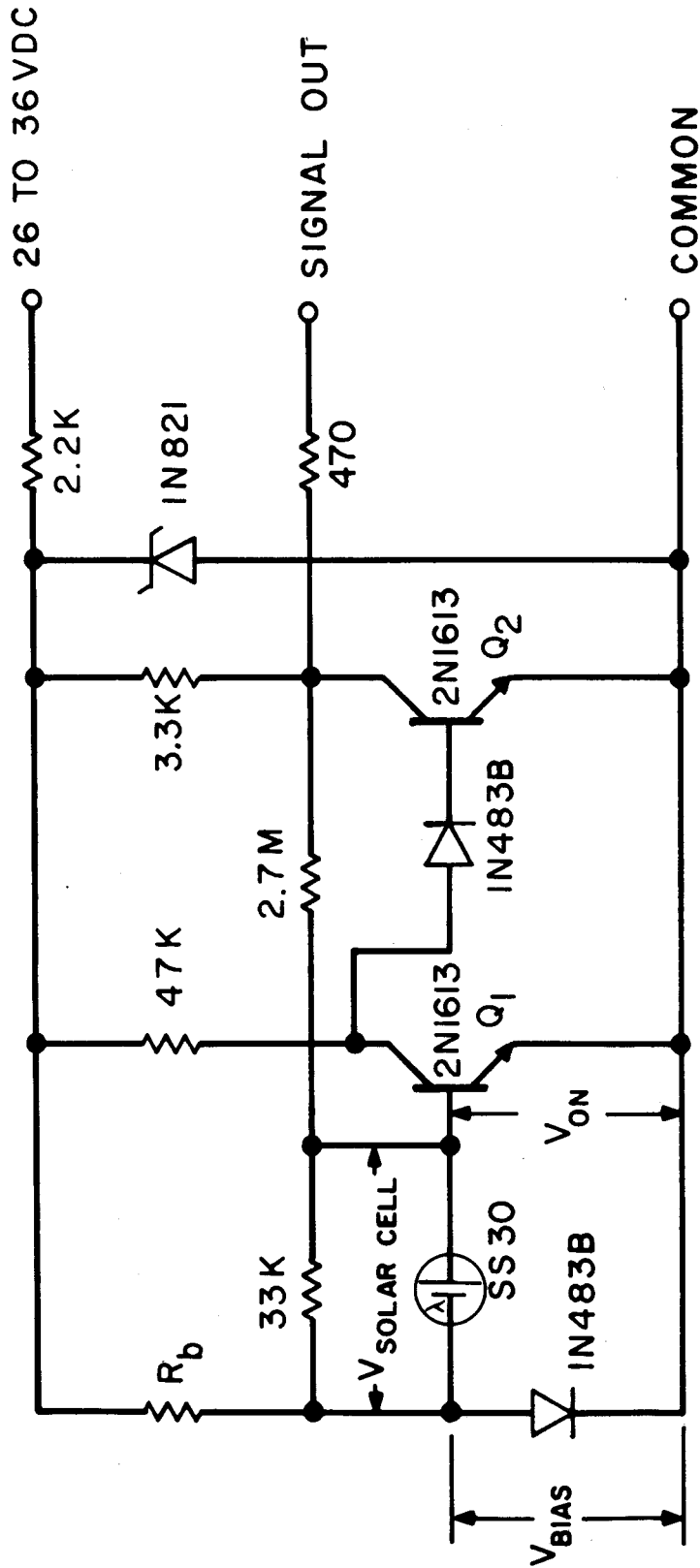(SS-30) as a function of (a) area and (b) temperature.

Figure 6. Circuit of solar aspect sensor.

14
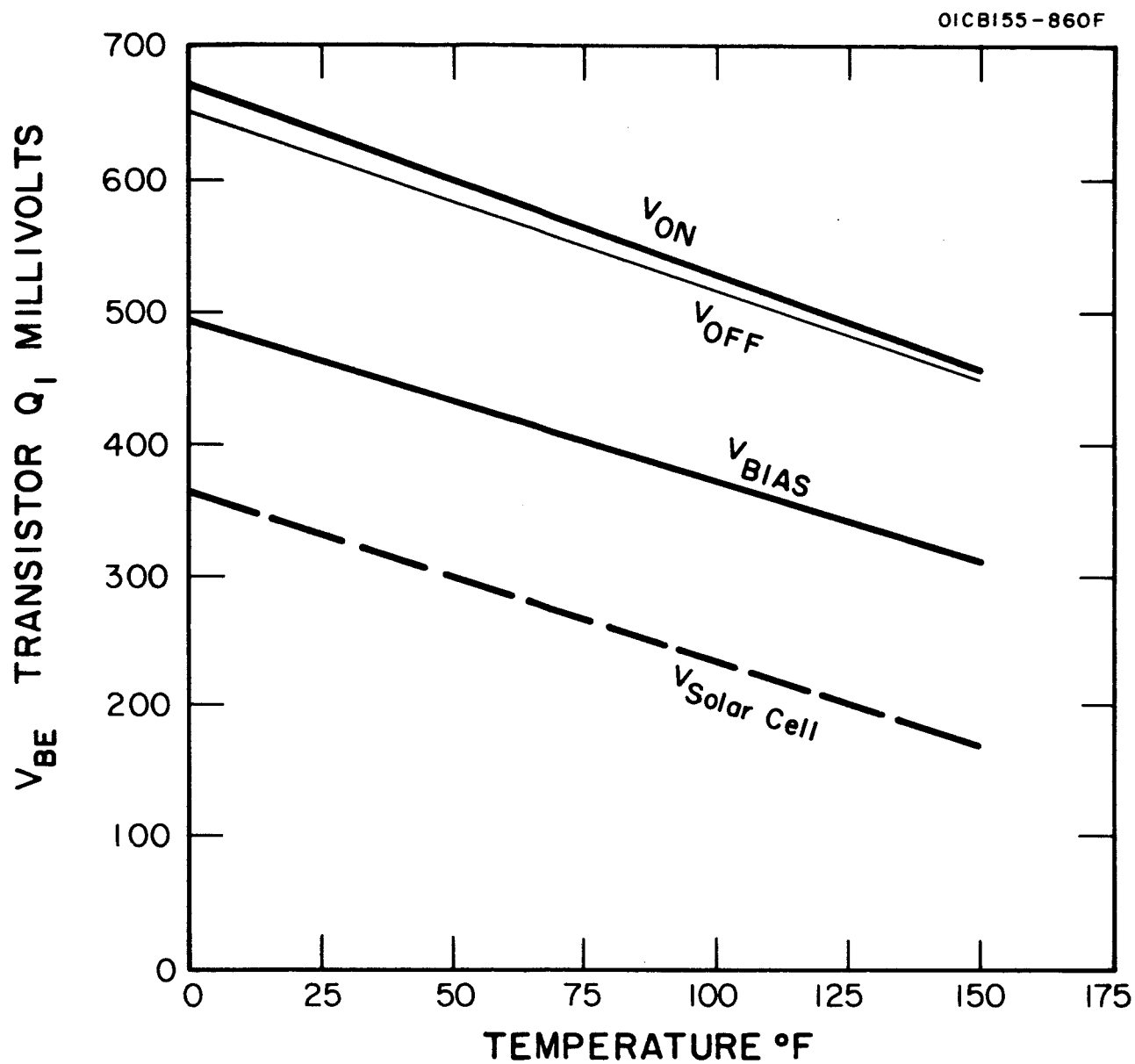
Figure 7. Effect of temperature on the switching circuit.

illustrates the data of a solar energy convertor with high sensitivity which has a temperature characteristic very similar to that of the input transistor. V_{bias}, the diode voltage, is set at a level that insures turn-on when the cell is illuminated by direct sunlight, but one which is low enough to prevent turn-on from background or reflected light. Positive switching action is achieved by feedback through the 2.7 megohm resistor.

CONSTRUCTION

An exploded view of the assembly shown in Figure 8 pictures the three main parts of the instrument: (1) the front and rear aperture plates and the self-locating spacers, (2) the solar energy convertor, and (3) the wave shaping circuit.

The self-locating spacers, machined to a tolerance of ±0.0005 inch, serve two purposes: (1) to position the center of the rear aperture plate which masks down the solar energy convertor squarely behind the center of the diamond shaped aperture, and (2) to fix the exact distance between the plates as determined by the fixed parameters, α_m, ϕ_o and the height of the diamond shaped aperture. Since this mechanical arrangement precisely fixes the geometry, the accuracy of the sensor depends on the mechanical tolerances of the components. To insure negligible mechanical errors in the aperture plates, the original layouts are drawn ten times size and reduced optically to make the negative. The front and rear aperture plates are fabricated from Kodak Photoplast Plate, a clear, rigid acrylic plastic material 0.060 inch thick, which supports a photographic emulsion. The Photoplast Plate is exposed by a contact process.

The solar cell is mounted on the back of the rear aperture plate. Since the convertor is rather brittle, special precautions were taken to insure that it would withstand the rigorous environment of high performance rockets. The aspect sensor has been successfully tested for shock level of 100 g's for 11 milliseconds and vibration tests of 50 to 2000 cps at 20 g's.

The housing is fabricated from rectangular aluminum tubing. The configuration of the aspect sensor is shown in Figure 9. The overall size is 1-1/2" x 1-3/8" x 2", excluding the connector. The sensor is mounted by four tapped holes (6-32) in the base. The weight is 3.6 ounces. The power requirements are 10 ma at 26-38 volts DC. The sensor is designed to operate over an ambient temperature range of $25^\circ F$ to $125^\circ F$.
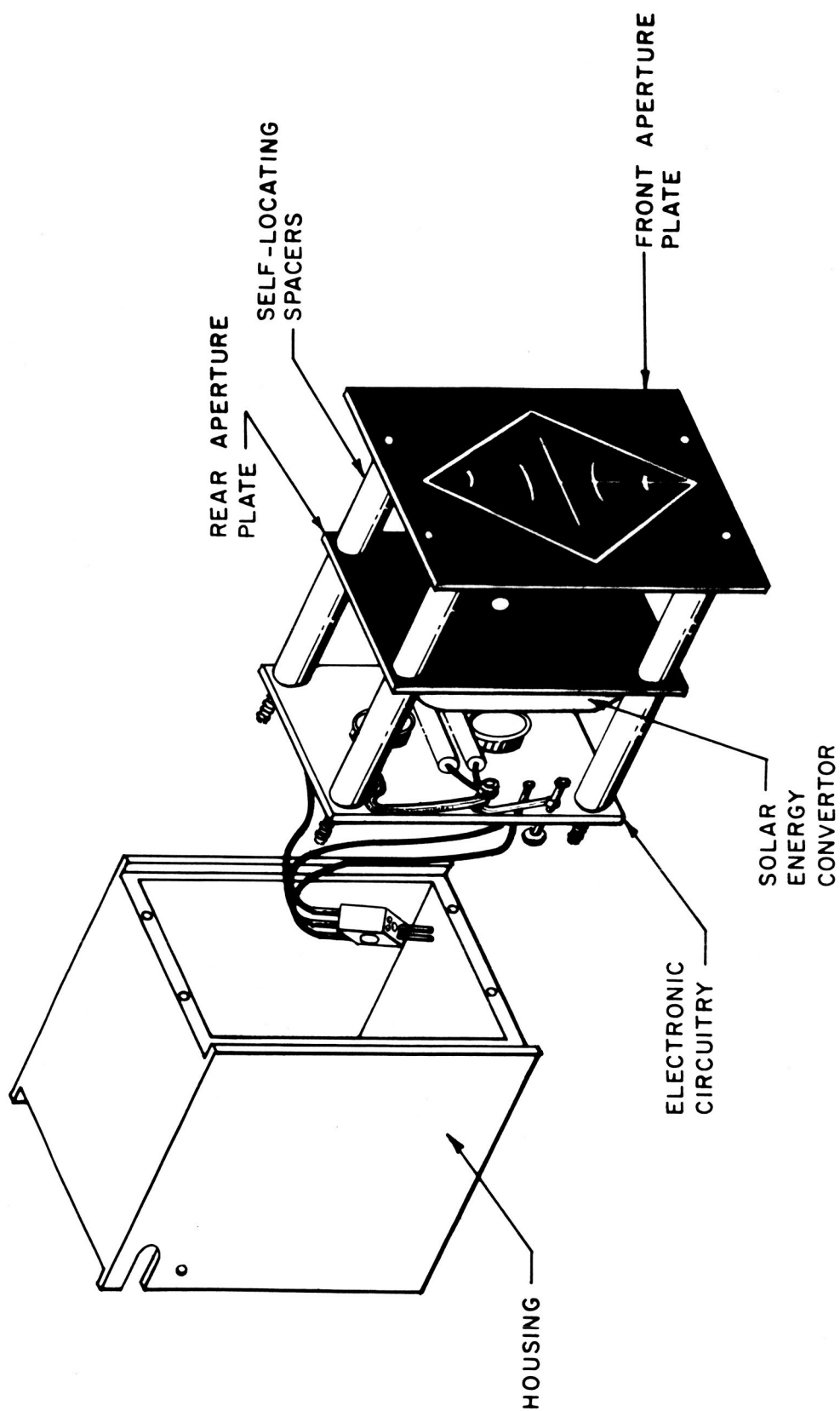
Figure 8. Exploded view of solar aspect sensor.

FRONT APERTURE PLATE

SELF-LOCATING SPACERS

REAR APERTURE PLATE

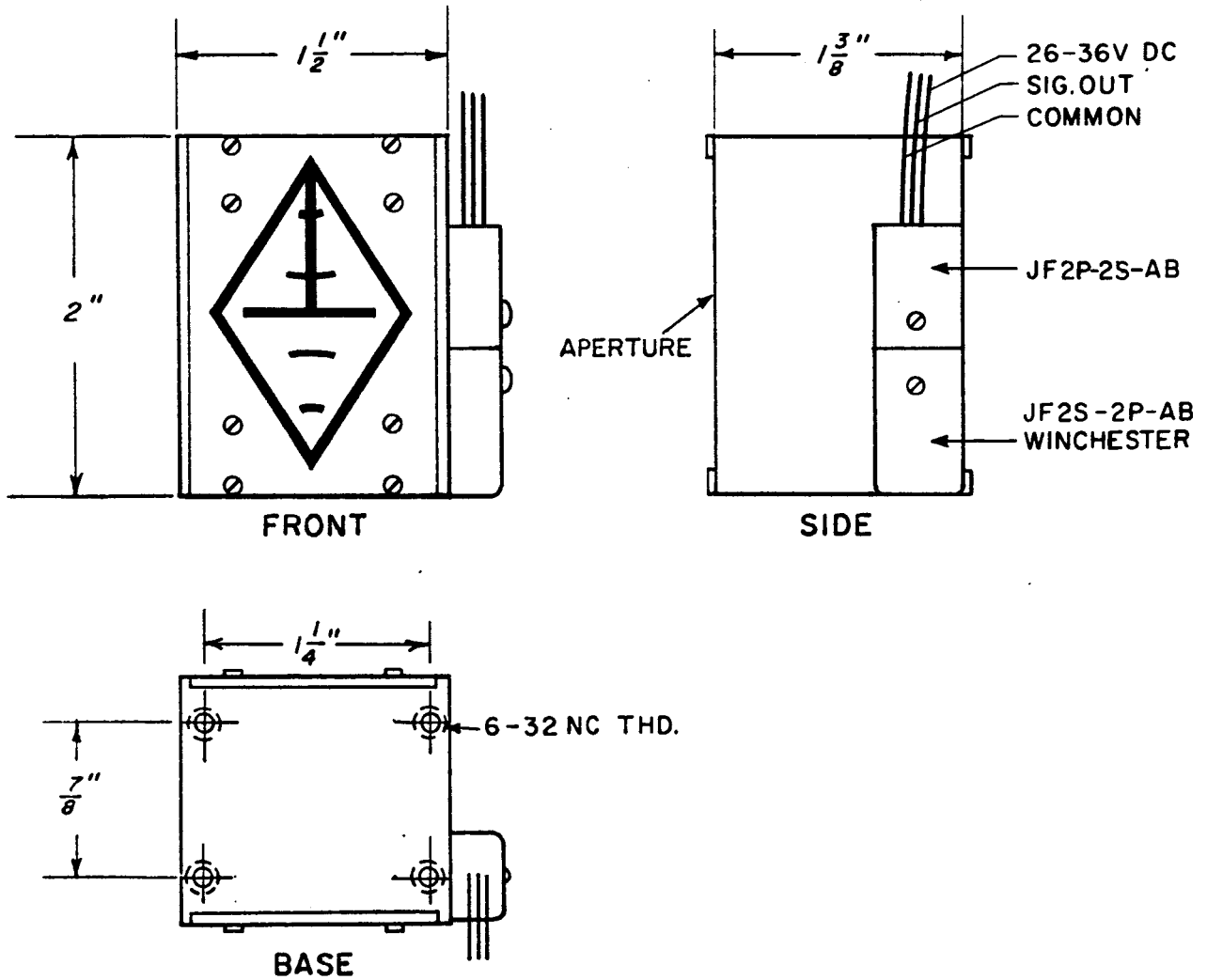SOLAR ENERGY CONVERTOR

ELECTRONIC CIRCUITRY

HOUSING

Figure 9. Solar aspect sensor configuration

APPLICATION AND DATA REDUCTION

Installation

A suggested arrangement of instrumentation in a solar radiation sensor package is illustrated in Figure 10. The angle at which the solar radiation sensors are positioned is designed to provide the most favorable aspect angle, for the particular condition of the flight, but it is imperative that the solar aspect sensor be mounted with the long axis of the diamond-shaped aperture parallel to the longitudinal spin axis of the rocket. It must be located so as to have an unobstructed field of view of 120° in azimuth and 140° longitudinally. The complete payload is shown in Figure 11. The aperture plate and the windows of the solar radiation sensors are protected from aerodynamic heating by ejectable doors during the launch phase. It is preferable to locate the aspect sensor close to the radiation sensor with which it is being used. In this payload the sensor is mounted on the same azimuth directly below the UV ion chamber and X-ray Geiger counter.

The convention has been to let the positive aspect angles, denoted by the three-pulse signal, represent angles toward the forward direction of the rocket. When the aspect sensor is installed, a record should be made of which of the pulse sequences represents the forward direction of the rocket.

The output signal is conveniently telemetered as an analog voltage in the form of a pulse train. A bandwidth of 1200 cps is recommended for satisfactory reproduction of the pulse wave form. The use of a somewhat lower bandwidth (e.g., 660 cps) will result in a significant delay of the pulse train, but accurate values of aspect angle can still be obtained.

Data Reduction

The time interval measurements t, t_o and the spin period t_s can easily be obtained with the required accuracy from a chart record having a speed of 10 inches per second. A typical 10 in/second telemetry record from the eclipse series is shown in Figure 12. The data from two Lyman-α ion chambers augmented by two solar aspect sensors is illustrated as an example for the following discussion on data reduction.

21

LONGITUDINAL
SPIN AXIS

DUAL DOOR
EJECTION
MECHANISM

DOOR

LONG AXIS OF
DIAMOND SHAPED
APERATURE

ASPECT
SENSOR

HIGH VOLTAGE
POWER SUPPLY
& PULSE
CIRCUITRY

LYMAN
ALPHA

LYMAN
ALPHA
ELECTROMETER

DOOR

RADIOACTIVE
SOURCE

GEIGER
COUNTER

LYMAN
ALPHA

LONG AXIS OF
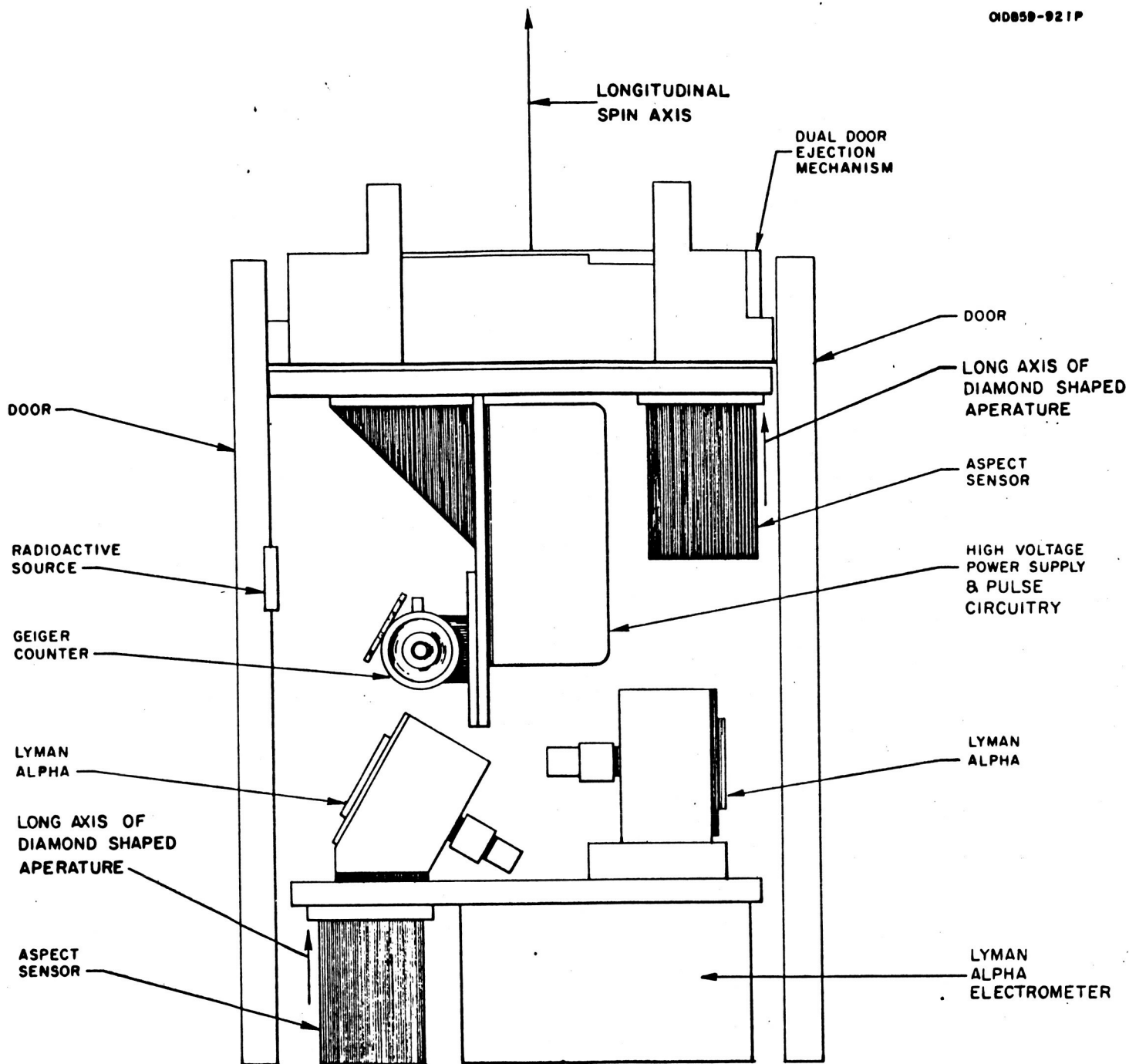DIAMOND SHAPED
APERATURE

ASPECT
SENSOR

Figure 10.   Arrangement of instrumentation in a solar
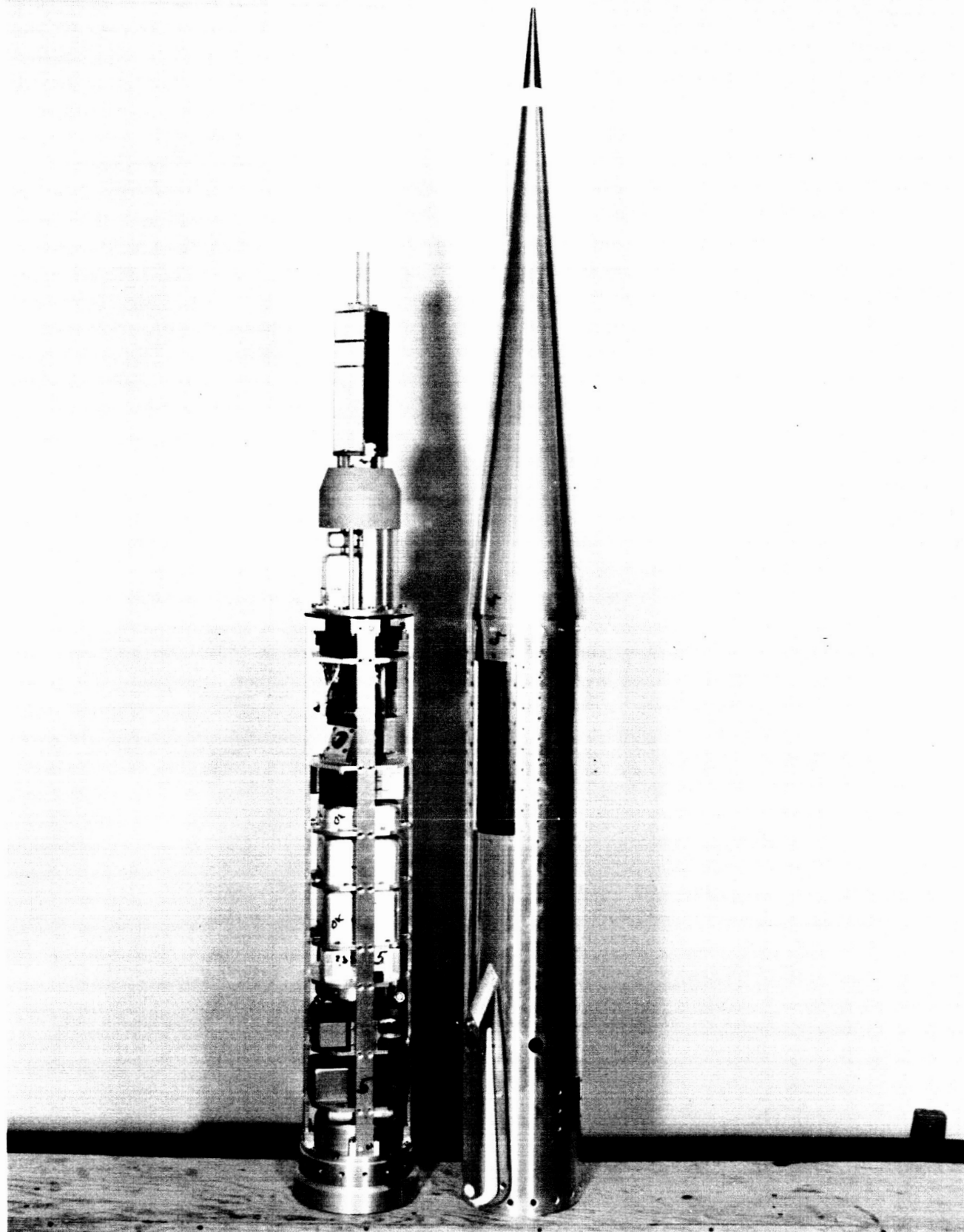radiation package.

22

Figure 11. One of six Nike-Apache payloads launched during
the solar eclipse of 20 July 1963 at Fort Churchill.

Equation (2) defines the aspect angle α for the condition of a line aperture. Since the slits of the diamond shaped aperture have a finite width (0.040 inch), the time interval t must be measured to the centers of the first and last pulses, or, more conveniently, to the leading edges of the extreme pulses as indicated in Figure 12. The spin period t_s is also measured.

Then the angle ϕ is give by:

$$\phi = 180 \frac{t}{t_s} \text{ degrees}$$

The angle ϕ_o is given as 60°, thus

$$\frac{\phi}{\phi_o} = 3 \frac{t}{t_s} \quad .$$

Then the aspect angle α is obtained directly from Figure 3, the calibration curve. The angle ϕ_o can also be obtained from the flight record. The three portions of Figure 12 show the vehicle turning over from a nose up to nose down during descent. A point of zero aspect angle is readily identified by the long central pulse. Measurement of t_o and t_s at this point immediately gives ϕ_o as

$$\phi_o = 180 \frac{t_o}{t_s} \text{ degrees}.$$

Vehicle Motion

Examples of the use of the solar aspect sensor to measure the precessional motion of a rocket are shown in figures 13, 14 and 15. Nike-Apache 14.143, Figure 13, was an extremely well stabilized vehicle in which no precessional motion could be detected by the sensor showing that the included angle of the precession cone was less than 2 degrees. The spin rate of this vehicle was 6.2 rps. Nike-Apache 14.94, Figure 14, is more typical of a spin-stabilized vehicle. A precession cone of 6.5 degrees included angle is indicated and the period of the precessional motion is 55 seconds. The vehicle spin rate was 4.1 rps. Nike-Apache 14.87, Figure 15, shows a large precessional motion in which the included angle of the cone is determined to be 173 degrees and the period is 12 seconds. The vehicle spin rate was 1.65 rps.

This last case illustrates the ambiguity resulting from the use of a single aspect sensor, whether solar or magnetic. If, as shown in Figure 16, the angle between the rocket axis and the reference
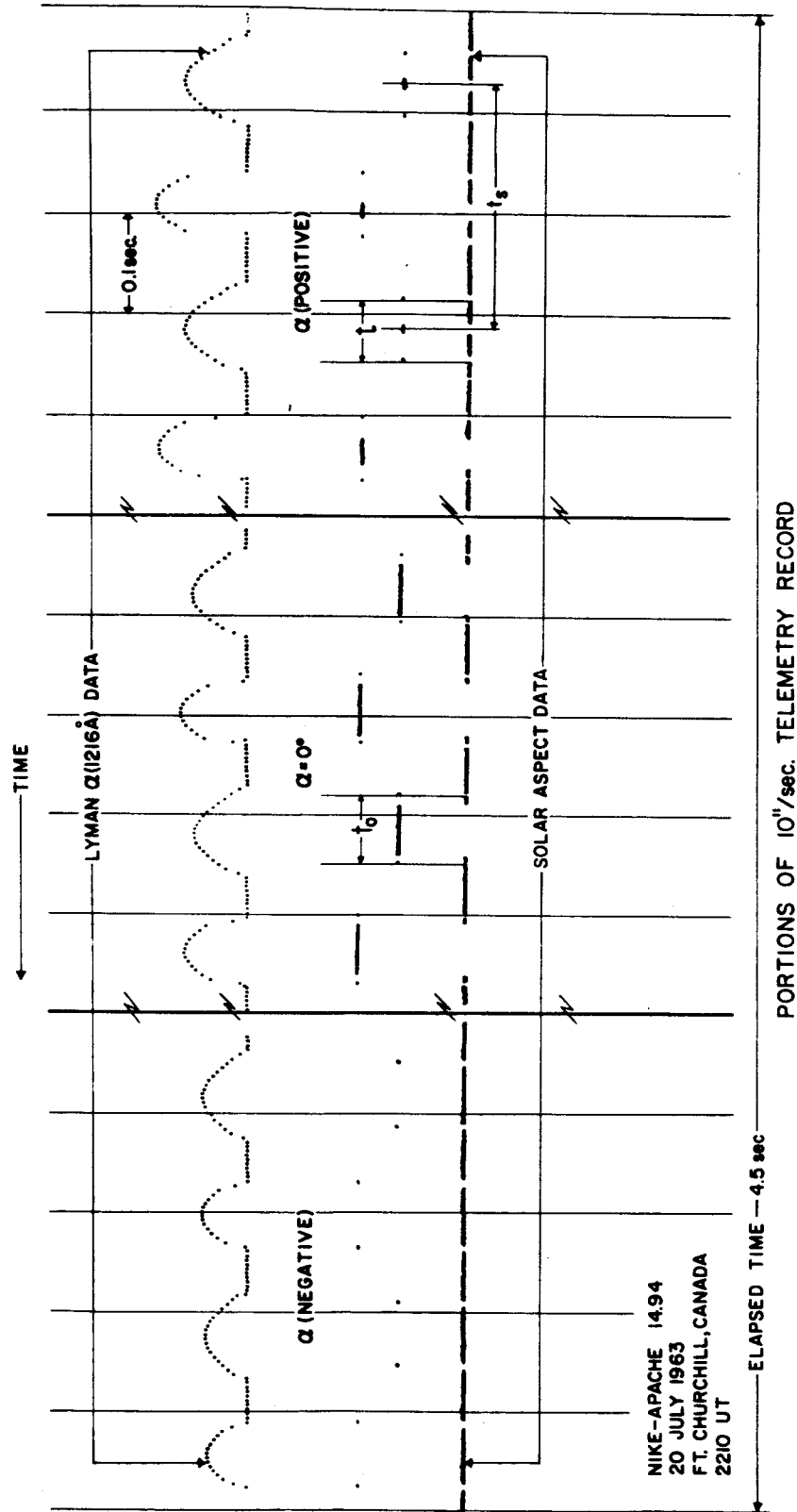
Figure 12. Solar aspect sensor data indicates vehicle turning over during descent from nose up to nose down attitude.
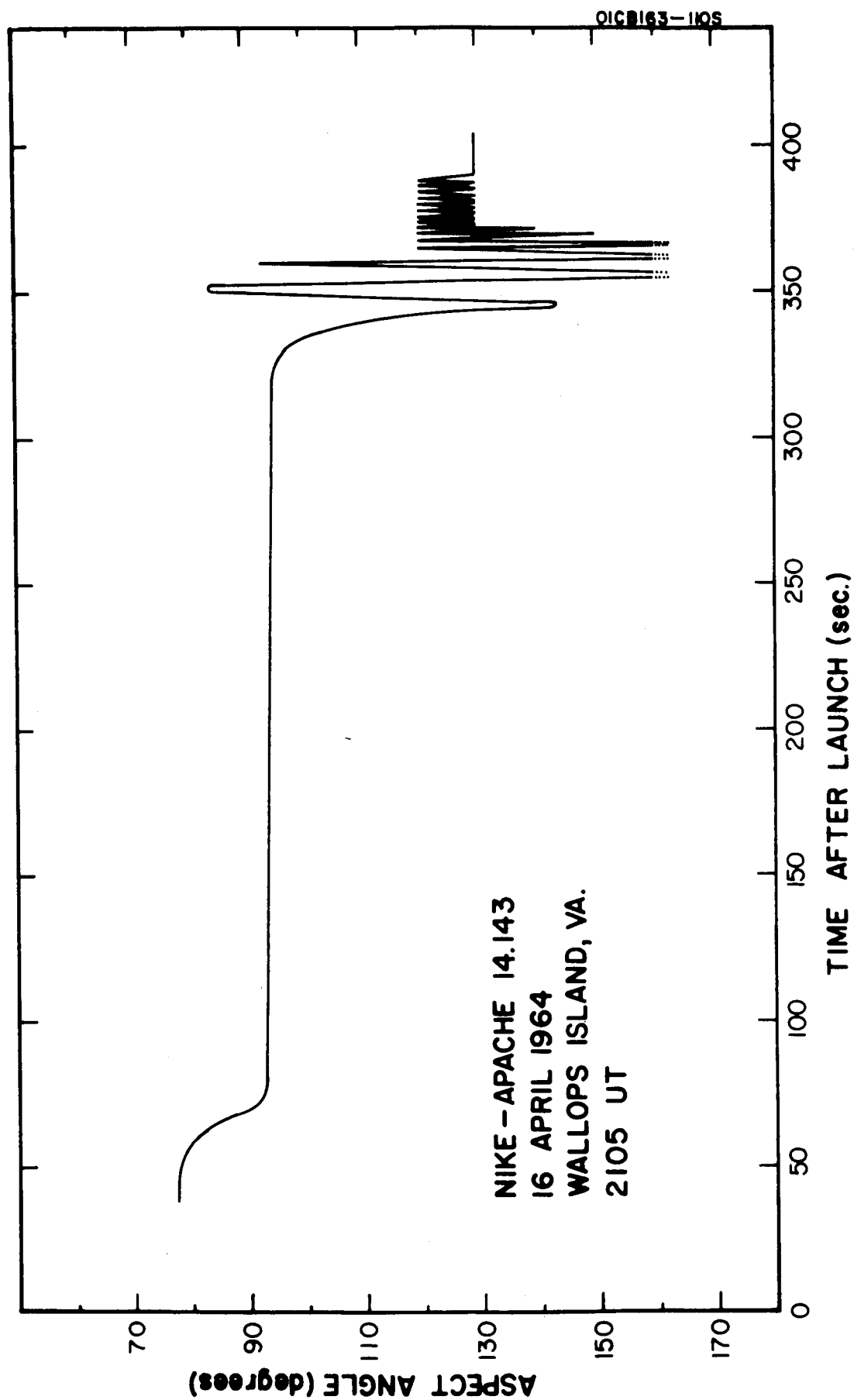
25

Figure 13. Time history of aspect angle for vehicle showing absence of precessional motion.
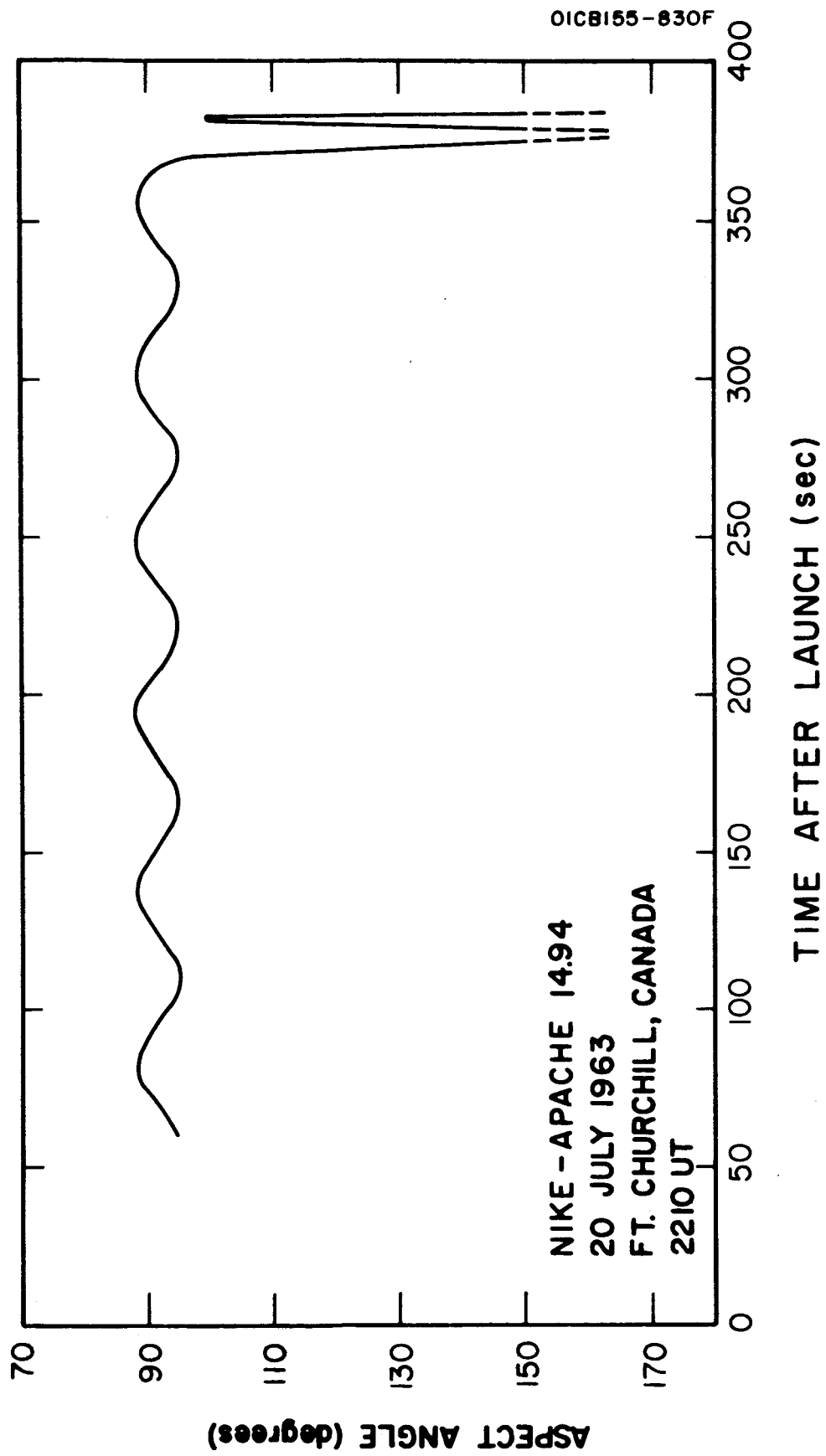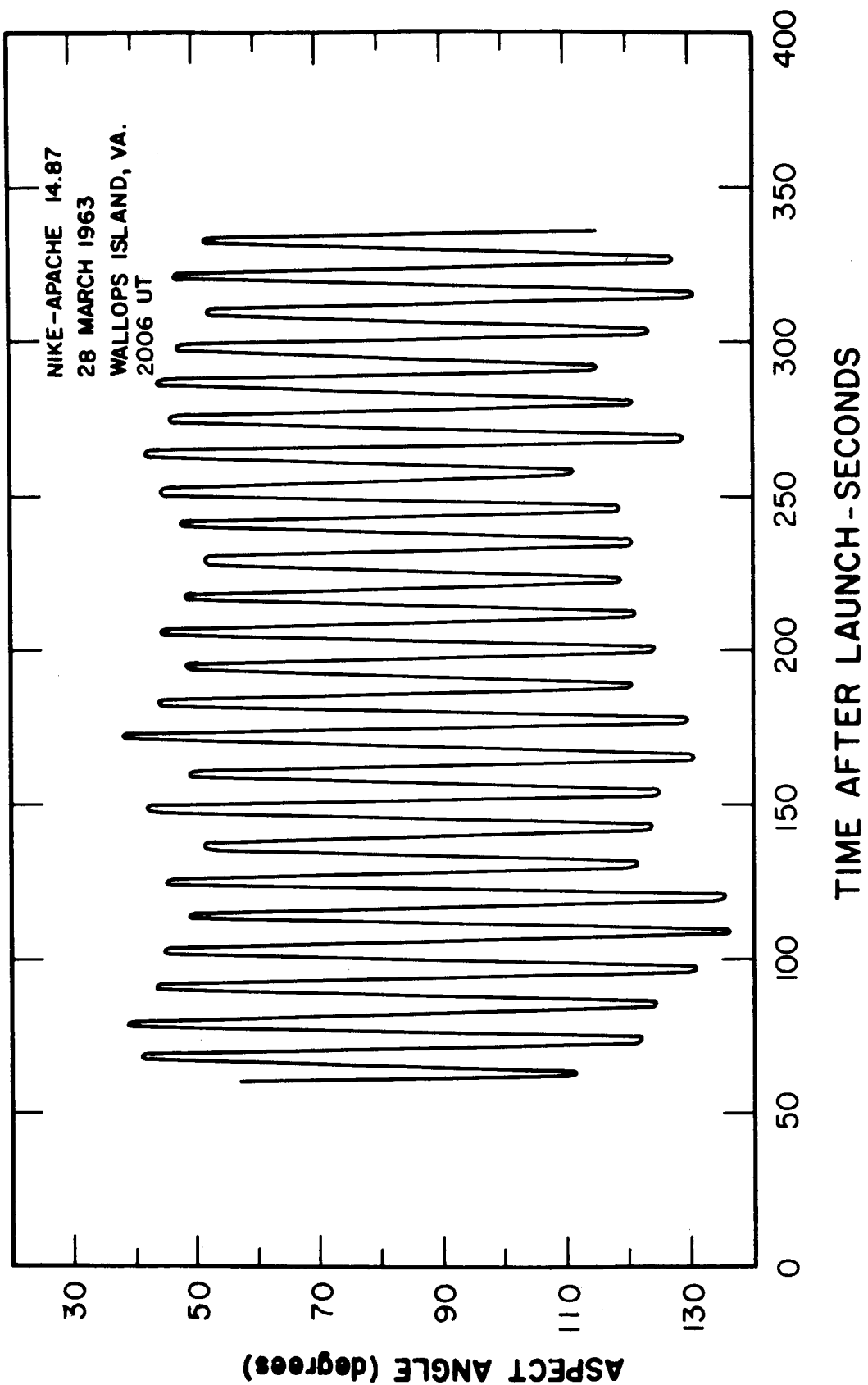
NIKE — APACHE 14.143
16 APRIL 1964
WALLOPS ISLAND, VA.
2105 UT

26

OICBI55-830F

NIKE-APACHE 14.94
20 JULY 1963
FT. CHURCHILL, CANADA
2210 UT

TIME AFTER LAUNCH (sec)

ASPECT ANGLE (degrees)

Figure 14. Time history of aspect angle for vehicle showing small precession cone.

NIKE-APACHE 14.87
28 MARCH 1963
WALLOPS ISLAND, VA.
2006 UT

TIME AFTER LAUNCH-SECONDS

ASPECT ANGLE (degrees)

Figure 15. Time history of aspect angle for vehicle showing large precession cone.
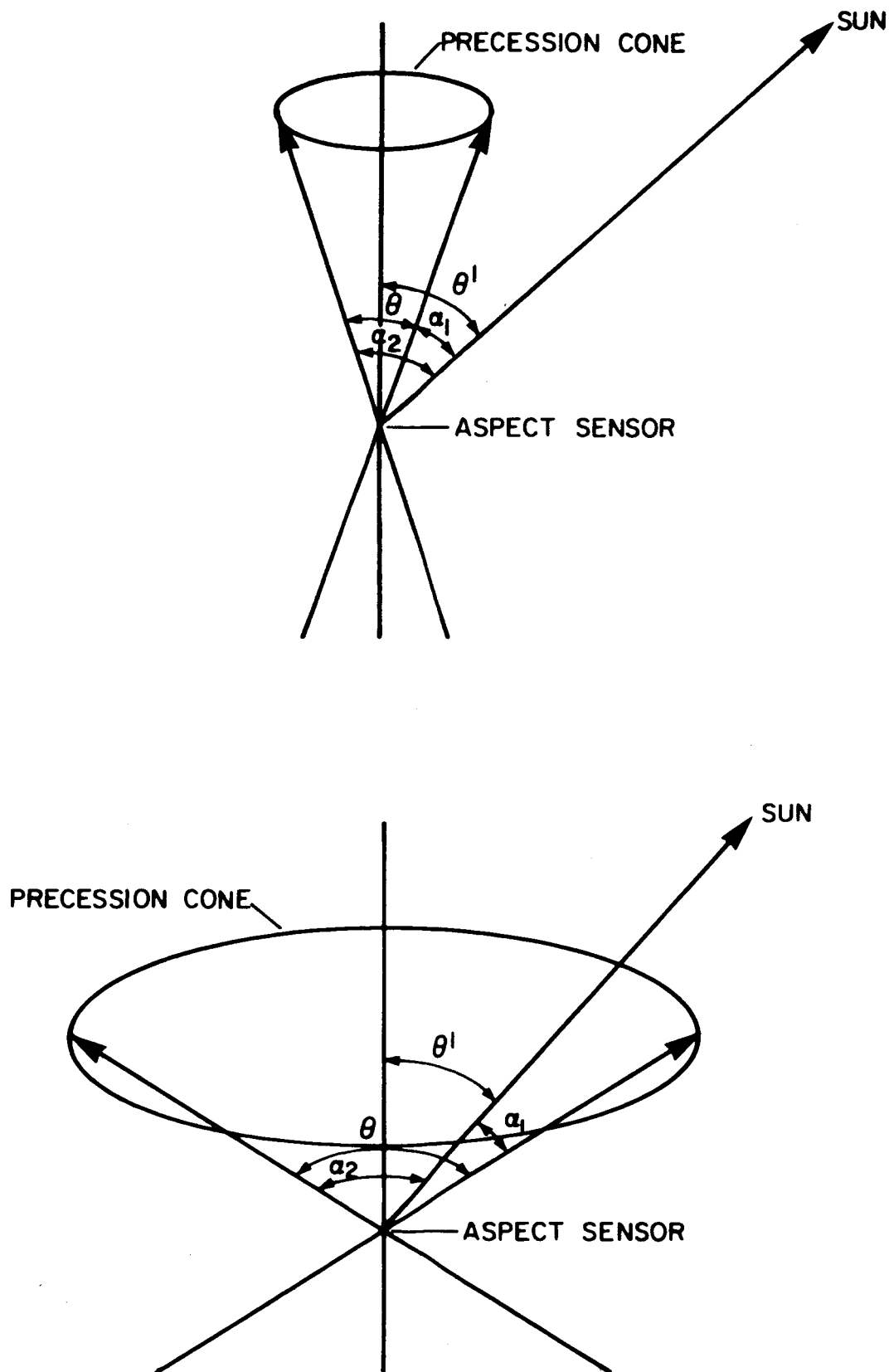
28

Figure 16. Ambiguity of precession cone resulting from the use of a single aspect sensor.

29

direction varies between a minimum value α_1 and a maximum value α_2, the included angle of the precession cone can have two values: for small cone $\theta = \alpha_2 - \alpha_1$; for the large cone $\theta = \alpha_2 + \alpha_1$.

The ambiguity can be resolved in some cases where the angle θ' between the rocket velocity vector and the reference direction is known (for example from radar data). For the small cone $\theta' = (\alpha_2 + \alpha_1)/2$ and for the large cone $\theta' = (\alpha_2 - \alpha_1)/2$. In the case of Nike-Apache 14.87 it could be shown that the large cone gives the only possible solution.